

Design of supercurrent diode by vortex phase texture

Yuri Fukaya,^{1,2,*} Maria Teresa Mercaldo,³ Daniel Margineda,⁴ Alessandro Crippa,⁴
Elia Strambini,⁴ Francesco Giazotto,⁴ Carmine Ortix,³ and Mario Cuoco¹

¹*CNR-SPIN, I-84084 Fisciano (SA), Italy, c/o Università di Salerno, I-84084 Fisciano (SA), Italy*

²*Faculty of Environmental Life, Natural Science and Technology, Okayama University, 700-8530 Okayama, Japan*

³*Dipartimento di Fisica “E. R. Caianiello”, Università di Salerno, IT-84084 Fisciano (SA), Italy*

⁴*NEST Istituto Nanoscienze-CNR and Scuola Normale Superiore, I-56127, Pisa, Italy*

We investigate supercurrent nonreciprocal effects in a superconducting weak-link hosting distinct types of vortices. We demonstrate how the winding number of the vortex, its spatial configuration, and the shape of the superconducting lead can steer the sign and amplitude of the supercurrent rectification. We find a general criterion for the vortex pattern to maximize the rectification amplitude of the supercurrent. The underlying strategy is the search for specific vortex core positions yielding a vanishing amplitude of the supercurrent first harmonic. We also prove that supercurrent nonreciprocal effects can be used to diagnose high-winding vortex and to distinguish between different types of vorticity. Our results thus provide a toolkit to control the supercurrent rectification by means of vortex phase textures and nonreciprocal signatures to detect vortex states with nonstandard phase patterns.

Introduction. Vortices represent fundamental topological excitations in superfluid and superconductors. They have been predicted and successfully observed in a broad range of systems including superconductors [1], liquid helium [2–4], ultracold atomic gases [5], photon fields [6], and exciton-polariton condensates [7, 8]. Vortices are generally characterized by a quantized phase-winding and a suppressed order parameter at their core. A gradient of the phase ϕ of the superconducting order parameter $\Delta = |\Delta| \exp(i\phi)$ yields a circulating supercurrent around the core of the vortex whereas the amplitude is vanishing, i.e. $|\Delta| \rightarrow 0$. For conventional superconductors, due to the single-valuedness of the superconducting order parameter, the winding number associated with the phase gradient is forced to be an integer V_0 . In principle, V_0 can assume values larger than one. Apart from having V_0 vortices with winding number equal to one, a giant vortex with winding number V_0 can also realize. A giant vortex is expected to be relevant in small superconductors with confined geometries. To date, probing of such unconventional vortex state has been mostly addressed by magnetic means in suitably tailored geometric configurations, e.g. by Hall probe [9–11] and scanning SQUID microscopy [12], or by tunneling microscopy and spectroscopy [13–17].

Here, we unveil a specific relation between the occurrence of vortex states with any given winding number in a Josephson weak-link and the rectification of the supercurrent flowing across the junction. Supercurrent rectification is a timely problem at the center of intense investigation [18–24]. A large body of work devoted to supercurrent rectification focuses on superconducting states marked by linear phase gradients with, for instance, Cooper pair momentum [25–27] or helical phases [28–32], as well as screening currents [33, 34], and supercurrent related to self-field [35, 36] or back-action mechanisms [37]. Vortices or circular phase gradients, associ-

ated to conventional winding, are also expected to yield supercurrent diode effects, due to the induced Josephson phase shift [38], and their role has been investigated for a variety of physical configurations [36, 39–48]. However, whether and how superconducting phase patterns with nontrivial winding for the vorticity can be probed by nonreciprocal response, are problems not yet fully uncovered.

By studying nonreciprocal supercurrent effects arising from distinct types of vortex phase texture in Josephson weak-links, we show that while a superconducting phase with vortices can generally lead to nonvanishing supercurrent rectification, the sign and amplitude of the rectification in the Josephson diode effect can be manipulated by the position of the vortex core and the winding of the phase vortex. We thereby uncover a general criterion to single out which phase vortex configuration can maximize the rectification amplitude of the supercurrent. Our findings provide a general toolkit for the design and control of supercurrent rectification by vortex phase texture.

Model. We consider a planar superconducting weak-link with the geometry shown in Fig. 1 (a). For convenience, the system size is expressed as $L_y \times (L_x^L + L_x^N + L_x^R)$ with L_y being the lateral thickness, $L_x^{L,R,N}$ the width in the left (L), right (R) and normal (N) region of the superconducting weak-link, respectively. The superconducting order parameter on the left and right side of the junction is given by $\hat{\Delta}_{L,R} e^{i\varphi_{L,R}}$. Then the Hamiltonian can be written as

$$\hat{H} = \sum_{\langle x,y;x',y' \rangle} \hat{C}^\dagger(x,y) \hat{H}(x,y;x',y';\varphi) \hat{C}(x',y'), \quad (1)$$

with φ being the phase difference between the order parameters across the junction, $\varphi = \varphi_L - \varphi_R$, and $\mathbf{r} = (x,y)$ labelling the site position. Here, $\langle x,y;x',y' \rangle$ indicates the nearest-neighbor sites for electrons hopping processes

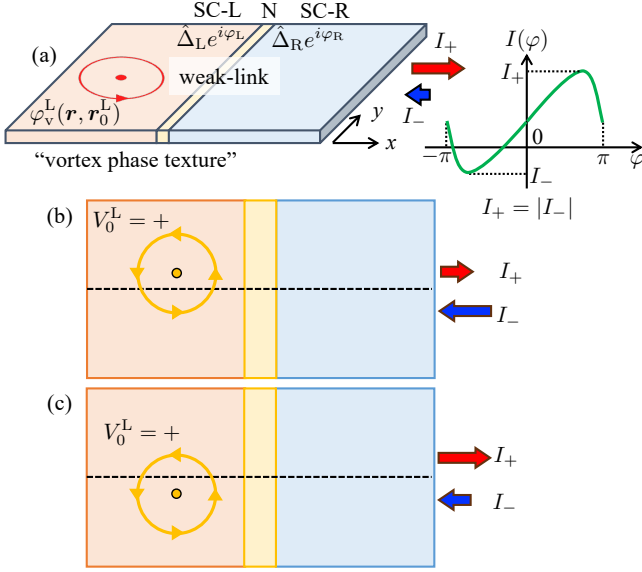


FIG. 1. (a) Schematic of the Josephson junction with a representative nonreciprocal current phase relation. (b)(c) Sketch of the superconducting weak link with a vortex placed on the left side of the junction. We show two representative vortex positions along the lateral direction. Since the supercurrent pattern is spatially modified by the phase vortex, it can become nonreciprocal, i.e. the forward supercurrent I_+ is different from the backward one I_- . The vortex winding, V_0^L , can take any integer number l .

and $\hat{C}^\dagger(x, y) = [c_{x,y,\uparrow}^\dagger, c_{x,y,\downarrow}^\dagger, c_{x,y,\uparrow}, c_{x,y,\downarrow}]$ denotes the operator in the electron-hole space for the spin up and down configuration at a given position (x, y) . We consider a conventional pairing with spin-singlet s -symmetry and assume a representative value for the junction transparency, i.e. $t_{\text{int}} = 0.90$. A variation of the amplitude of t_{int} does not qualitatively change our results.

To investigate the rectification properties of the supercurrent in the junction, we consider a single vortex configuration assuming a variable winding number and core position as shown in Figs. 1 (b,c). The vortex is placed in the left side of the junction but the results for vortices on the right side of the junction can be simply obtained using that inversion symmetry leads to a sign variation of the rectification amplitude [see Supplemental Material (SM) [49]]. Antivortex configurations through mirror and time-reversal transformations can be also directly deduced from the results of the single vortex (see SM [49]). Here, we consider vortices that remain pinned and are not set in motion by the flow of supercurrent. The presence of vortex flow would introduce dissipative effects and nonreciprocal phenomena related to the motion of the vortices, which is beyond the aim of the present study.

To simulate the vortex state with the core at a given position, $\mathbf{r}_0^L = (x_0^L, y_0^L)$, the phase value at \mathbf{r} in the left-

side superconductor is given by

$$\varphi_v^L(\mathbf{r}, \mathbf{r}_0^L) = V_0^L \arg[(x - x_0^L) + i(y - y_0^L)], \quad (2)$$

with V_0^L being the winding number of the vortex. $\varphi_v^L(\mathbf{r}, \mathbf{r}_0^L)$ reverses its sign by changing the sign of V_0^L , and $|V_0^L|$ corresponds to the number of sign changes in the real space \mathbf{r} for the phase value when winding around the core of the vortex. Here, to deal with the boundary condition along the lateral direction, we employ the method of image vortices to achieve a vanishing component of the supercurrent perpendicular to the lateral edges of the junction (see SM [49]). The vortex phase texture related to the above boundary conditions is indicated as $\tilde{\varphi}_v^L(\mathbf{r}, \mathbf{r}_0^L)$. The pair potential Δ_L and Δ_R for spin-singlet s -wave state are given by $\Delta_L = |\Delta_0| \tilde{\Theta}(\mathbf{r}, \mathbf{r}_0^L) e^{i\tilde{\varphi}_v^L(\mathbf{r}, \mathbf{r}_0^L)}$ and $\Delta_R = |\Delta_0|$ with $|\Delta_0|$ being the superconducting energy gap amplitude. In the presence of a phase vortex texture, the amplitude of the pair potential Δ_L is modified by $\tilde{\Theta}^L(\mathbf{r}, \mathbf{r}_0^L)$ for each position \mathbf{r} : $\tilde{\Theta}^L(\mathbf{r}, \mathbf{r}_0^L) = \tanh[|\mathbf{r} - \mathbf{r}_0^L|/\xi_0^L]$, with ξ_0^L being the vortex size.

The current phase relation of the Josephson current is obtained by evaluating the variation of the free energy F with respect to the phase bias across the junction: $I(\varphi) \propto \partial F(\varphi)/\partial \varphi$ (see SM [49]). The computational analysis is performed at zero temperature, but a thermal change does not alter qualitatively the results. For our purposes, we recall that if time-reversal is broken then the supercurrent can be expanded in even and odd harmonics with respect to the phase bias variable as $I(\varphi) = \sum_m [I_m \sin(m\varphi) + J_m \cos(m\varphi)]$ [50]. To assess the nonreciprocal supercurrent due to the presence of the vortex in the junction, we evaluate the rectification amplitude η that is conventionally expressed as $\eta = \frac{I_+ - |I_-|}{I_+ + |I_-|}$, with $I_{+(-)}$ the maximum amplitude of the supercurrent for forward (backward) directions, respectively. For the presented results, we set the energy gap amplitude as $|\Delta_0| = 0.02t$ (t is the electron hopping amplitude), the maximum Josephson current value, without vortex, as $I_0 = 0.012|\Delta_0|$, and the size of the superconducting leads as $L_x^L = L_x^R = aL_y$ with a being the aspect ratio setting out a square or rectangular shape of the superconductors in the junction. The computation is performed for $L_y = 30$, and $\xi_0^L = 10$ for the size of the vortex core. A variation of these lengths does not affect the results, thus, for clarity, we introduce the reduced coordinates (\tilde{x}, \tilde{y}) in the Josephson junction [Fig. 2 (a)] (see details in Sect. I of SM [49]).

Nonreciprocal supercurrent: vortex core position and winding number. In Figs. 2 (b)-(m) we present the rectification amplitude for different values of the vortex winding and by varying the vortex core position assuming $a = 3/2$ as representative cases for the aspect ratio of the superconducting lead. The analysis for all vortex winding is performed by scanning the vortex core position within

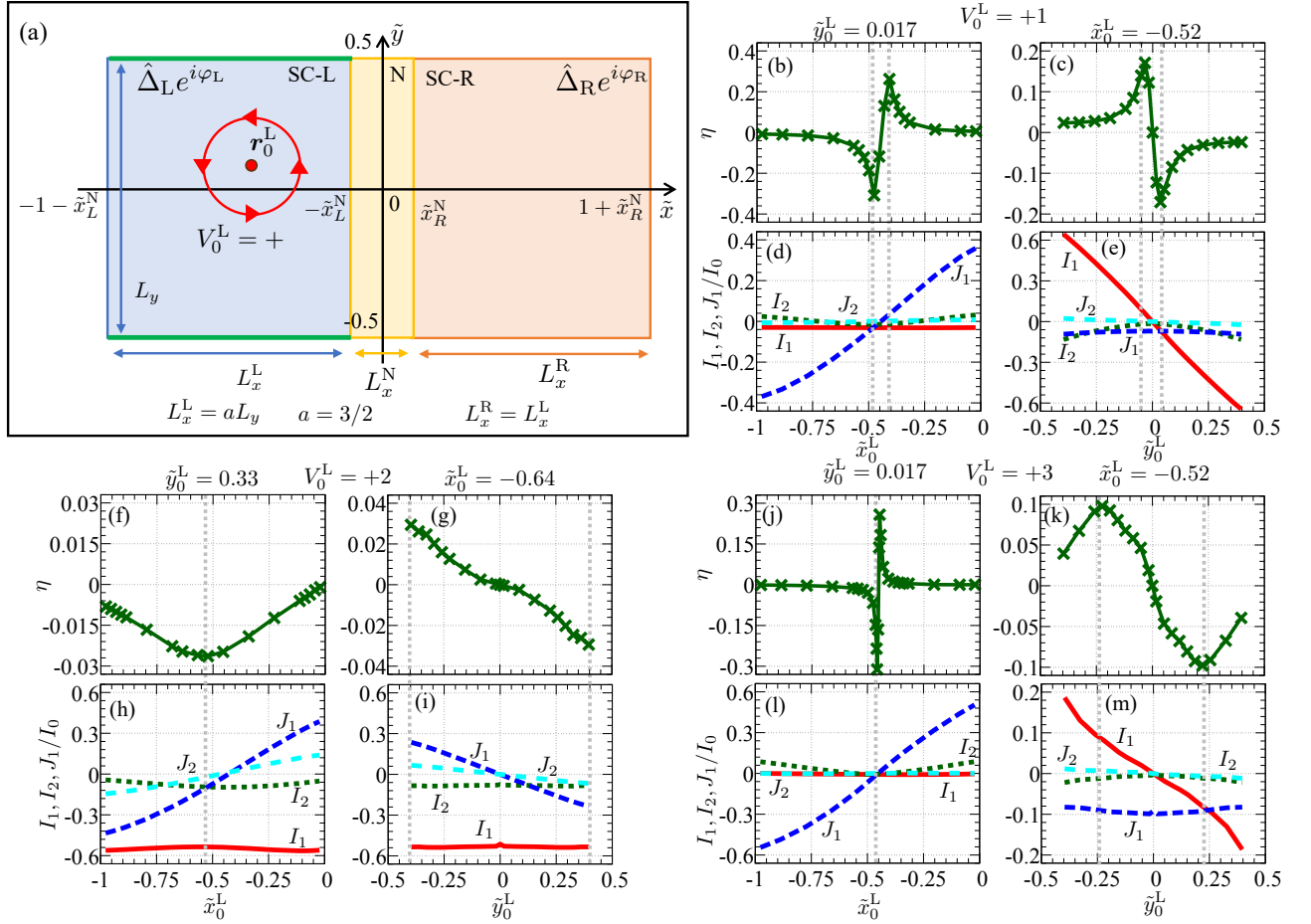


FIG. 2. (a) Schematic illustration of the Josephson junction with reduced coordinates. At the edges (green lines) we assume that the component of the supercurrent perpendicular to the boundary is vanishing. The analysis is performed for a vortex configuration having winding number $V_0^L = +l$ with $l = 1, 2, 3$. Evolution of the rectification amplitude η with regard to the vortex core coordinates for different winding numbers: (b,c) $V_0^L = 1$, (f,g) $V_0^L = 2$, and (j,k) $V_0^L = 3$. Spatially resolved harmonics of the supercurrent: I_1 (red-solid line), I_2 (green-dotted), J_1 (blue-dashed), and J_2 (cyan-dashed) indicate the odd-parity first harmonic, the odd-parity second harmonic, the even-parity first harmonic, and the even-parity second harmonic amplitude, respectively. Longitudinal scan: I_1 , I_2 , J_1 , and J_2 at a given \tilde{y}_0^L as a function of \tilde{x}_0^L for (d) $V_0^L = 1$, (h) $V_0^L = 2$, and (l) $V_0^L = 3$. Lateral scan: I_1 , I_2 , J_1 , and J_2 at a given \tilde{x}_0^L as a function of \tilde{y}_0^L for (e) $V_0^L = 1$, (i) $V_0^L = 2$, and (m) $V_0^L = 3$. The gray dotted lines refer to the position of the maximal rectification and are a guide to indicate the values I_1 , I_2 , J_1 , and J_2 . We set \tilde{y}_0^L as (b)(d)(j)(l) 0.017 and (f)(h) 0.33, and \tilde{x}_0^L as (c)(e)(k)(m) -0.52 and (i)(m) -0.64 . The aspect ratio is $a = 3/2$. The maximal rectification η occurs for vortex core positions corresponding to a supercurrent with I_1 , I_2 , and J_1 components that are comparable in size. The sign change of η is related to the vanishing of I_1 and the zeros of J_1 when the amplitude is comparable to I_1 .

the superconducting lead along the longitudinal (x) and lateral direction y . We start by considering a conventional vortex with winding $V_0^L = 1$. The outcome of the study indicates that the rectification tends to vanish and changes the sign if the vortex core is placed at the crossing of the longitudinal lead and transverse mirror lines of the left superconducting lead [Figs. 2 (b,c)]. For the geometry of the junction, these symmetry lines correspond to the $\tilde{y} \sim 0$ and $\tilde{x} \sim -0.5$ axes. Other vortex core positions away from the symmetry lines give a negligible rectification. One can also observe that the maximum of the rectification occurs nearby these nodal points at a

distance that is set by the vortex core size ξ_0^L . The behavior of the supercurrent rectification can be understood by inspection of the amplitude of the first harmonics in the current phase relation. For instance, placing the vortex core along the longitudinal direction at a different distance from the interface we find that the value of the first even-parity harmonic (J_1) changes sign at $\tilde{x} = -0.5$ [Figs. 2 (d)]. The J_1 component sets out the amplitude of the spontaneous supercurrent induced by the presence of the vortex at zero applied phase bias (i.e. $\varphi = 0$). For such a position, one can observe that the even-parity first harmonic (J_1) and the odd-parity second harmonic (I_2)

components have a small amplitude and are comparable to that of I_1 . We also consider the even-parity second harmonic component (J_2) which is vanishing or comparable to the other harmonics in order to optimize the rectification amplitude (see SM [49]). Instead, regarding the evolution of η as a function of the lateral coordinate \tilde{y} we find that the sign change of η occurs nearby $\tilde{y} \sim 0$. Now, the sign reversal is guided by the first odd-parity harmonic term (I_1) in the current phase relation [Figs. 2 (e)]. Both the scan along the \tilde{x} and \tilde{y} directions indicate that the rectification amplitude is maximal (of the order of 30%) for vortex core positions \mathbf{r}_0^L that correspond to configurations for which the first harmonics of the supercurrent have comparable strength. This trend for maximal rectification of the supercurrent is a general expectation which can be directly deduced by the analysis of a Josephson system with current phase relation with generic but comparable amplitudes for I_1 , I_2 , and J_1 ([51] and see SM for details [49]).

Moving to even high-winding, $V_0^L = 2$, we find that the small amplitude of the rectification occurs [Figs. 2 (f,g)] because of the large value of I_1 compared to I_2 and J_1 [Figs. 2 (h,i)]. Inspection of the harmonics content of the current phase relation confirms that the sign change of the rectification amplitude η occurs (does not occur) when J_1 reverses its sign [Figs. 2 (i) (Figs. 2 (h))]. Let us then consider a vortex with odd high-winding number $V_0^L = 3$. For $V_0^L = 3$, we observe that the maximal values of the rectification amplitude occur for the vortex core position that is near (away from) the mirror lines of the superconducting lead [Figs. 2 (j) (Figs. 2 (k))]. The rectification can reach 30% amplitude and their profile are qualitatively similar to those for $V_0^L = 1$ [Figs. 2 (d,e,j,k)], due to the boundary condition.

The analysis indicates that a key element to maximize the rectification is represented by the search of vortex configurations for which the first harmonics (even and odd-parity) are concomitantly almost vanishing. This is a general rule to get large rectification [51] (see also SM [49]). To this aim, one can make an analytical analysis of the first harmonics by considering the direct process of Cooper pairs transfer across the junction as given by [50, 52]

$$\tilde{I}(\varphi, \mathbf{r}_0^L) \propto \int_{S_L} \text{Im}[\Delta_L(\mathbf{r}, \mathbf{r}_0^L) \Delta_R^*] d\mathbf{r}, \quad (3)$$

where S_L is the area of the left side superconductor (see Sect. 3 in SM). Taking into account the form of the superconducting order parameter we have that:

$$\begin{aligned} \tilde{I}(\varphi, \mathbf{r}_0^L) \propto & \int_{S_L} \tilde{\Theta}^L(\mathbf{r}, \mathbf{r}_0^L) \\ & \times [\sin \varphi \cos \tilde{\varphi}_v^L(\mathbf{r}, \mathbf{r}_0^L) + \cos \varphi \sin \tilde{\varphi}_v^L(\mathbf{r}, \mathbf{r}_0^L)] d\mathbf{r}. \end{aligned} \quad (4)$$

This relation is general and can be applied to any type of vortex phase texture. Here, from this expression, we

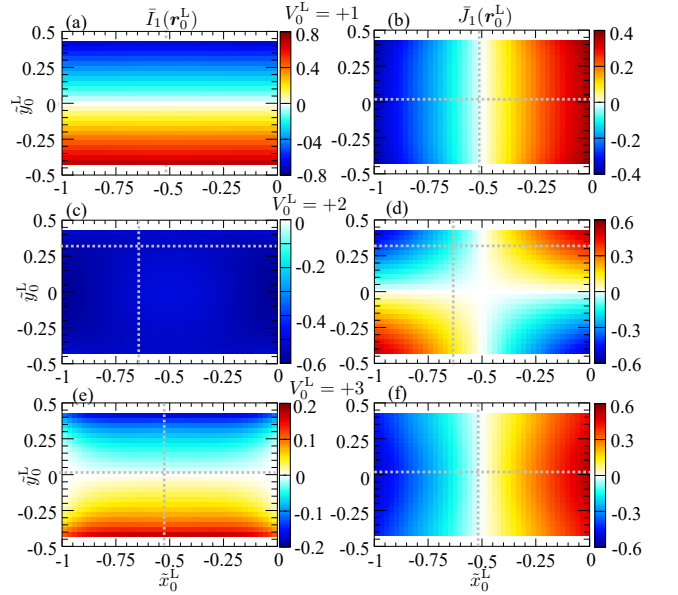


FIG. 3. Amplitude of the first harmonics of the Josephson current versus the vortex core positions for different vortex winding: (a,b) $V_0^L = 1$, (c,d) $V_0^L = 2$, (e,f) $V_0^L = 3$. I_1 and J_1 indicate the odd- and even-parity first harmonics of the supercurrent evaluated by the direct Cooper pairs tunneling. Gray-dotted and dashed lines stand for the vortex core positions, \tilde{y}_0^L and \tilde{x}_0^L , evaluated in Fig. 2. The aspect ratio is $a = 3/2$.

can deduce how nonreciprocal supercurrent directly links to the winding of the phase vortex. Focusing on the coefficients of $\sin \varphi$ and $\cos \varphi$, the structure of the vortex indeed directly impacts the even and odd-parity components of the first harmonics of the supercurrent. For convenience and in order to primarily extract the angular dependence of the harmonics content we neglect the amplitude variation in the vortex core. Hence, the effective first harmonics components $\bar{I}_1(\mathbf{r}_0^L)$ and $\bar{J}_1(\mathbf{r}_0^L)$ of \tilde{I} are substantially given by $\bar{I}_1(\mathbf{r}_0^L) = \int_{S_L} \cos \tilde{\varphi}_L(\mathbf{r}, \mathbf{r}_0^L) d\mathbf{r}$ and $\bar{J}_1(\mathbf{r}_0^L) = \int_{S_L} \sin \tilde{\varphi}_L(\mathbf{r}, \mathbf{r}_0^L) d\mathbf{r}$. We checked that the spatial variation of the superconducting order parameter in the core of the vortex does not alter the qualitative conclusions of the analysis. We find that their nodal lines can cross in different positions depending on the even and odd winding number [Fig. 3]. Due to the boundary condition, the same odd functions are qualitatively obtained for the odd winding number $V_0^L = 1, 3$ [Figs. 3 (a,b,e,f)]. Even functions without (with) the nodal structure for \bar{I}_1 (\bar{J}_1) are demonstrated at $V_0^L = 2$ [Figs. 3 (c,d)]. Finally, we have also considered the case of multiple vortices (see SM). Specifically, we have examined a scenario involving two vortices with the same winding (i.e. vortex-vortex) and two vortices with opposite winding (i.e. vortex-antivortex). The results indicate that the presence of a vortex-antivortex configuration generally suppresses the supercurrent rectification independently

of their relative position.

Conclusions. We have demonstrated that nonreciprocal supercurrents can be exploited to distinguish physical configurations with vortices having winding number equal to one, coexistence of vortices and antivortices or the occurrence of a giant vortex. A suitable platform to observe these effects can be based on Josephson junctions made of nanoislands in the presence of an applied magnetic field [13]. It is known that giant vortices can be induced by magnetic field for superconductors with coherence length much smaller than the magnetic penetration depth (e.g. Pb or Nb based nanostructures) [13]. Then, starting from a low magnetic field configuration with a vortex having, for instance, winding $V_0^L = 1$ nearby the center of the superconducting lead, the transition to a higher winding vortex state by the increase of the magnetic field will be accompanied to a sizable variation of the rectification. Detection of such transitions can be used to probe the high-winding vortex phase. Along this line, one can also envision a field-free platform [53] with circular current flow inducing high-winding vortices that concomitantly yield supercurrent rectification. Moreover, since a generic phase vortex texture can be expanded in harmonics by employing vortex configurations with different windings, then, in principle our results provide a toolkit to design the supercurrent rectification for a wide variety of superconducting phase patterns.

This work was funded by the EU's Horizon 2020 Research and Innovation Framework Program under Grant Agreement No. 964398 (SUPERGATE), No. 101057977 (SPECTRUM), by the PNRR MUR project PE0000023-NQSTI, by the PRIN project 2022A8CJP3 (GAMESQUAD), and by the MAECI project "ULTRA-QMAT".

* fukaya.yuri@spin.cnr.it

- [1] A. A. Abrikosov, On the Magnetic properties of superconductors of the second group, *Sov. Phys. JETP* **5**, 1174 (1957).
- [2] W. F. Vinen and D. Shoenberg, The detection of single quanta of circulation in liquid helium ii, *Proceedings of the Royal Society of London. Series A. Mathematical and Physical Sciences* **260**, 218 (1961).
- [3] G. P. Bewley, M. S. Paoletti, K. R. Sreenivasan, and D. P. Lathrop, Characterization of reconnecting vortices in superfluid helium, *Proceedings of the National Academy of Sciences* **105**, 13707 (2008).
- [4] L. F. Gomez, K. R. Ferguson, J. P. Cryan, C. Baccellar, R. M. P. Tanyag, C. Jones, S. Schorb, D. Anielski, A. Belkacem, C. Bernando, R. Boll, J. Bozek, S. Carron, G. Chen, T. Delmas, L. Englert, S. W. Epp, B. Erk, L. Foucar, R. Hartmann, A. Hexemer, M. Huth, J. Kwok, S. R. Leone, J. H. S. Ma, F. R. N. C. Maia, E. Malmerberg, S. Marchesini, D. M. Neumark, B. Poon, J. Prell, D. Rolles, B. Rudek, A. Rudenko, M. Seifrid, K. R. Siefertmann, F. P. Sturm, M. Swiggers, J. Ullrich, F. Weise, P. Zwart, C. Bostedt, O. Gessner, and A. F. Vilesov, Shapes and vorticities of superfluid helium nanodroplets, *Science* **345**, 906 (2014).
- [5] Z. Hadzibabic, P. Krüger, M. Cheneau, B. Battelier, and J. Dalibard, Berezinskii–kosterlitz–thouless crossover in a trapped atomic gas, *Nature* **441**, 1118 (2006).
- [6] L. Allen, M. W. Beijersbergen, R. J. C. Spreeuw, and J. P. Woerdman, Orbital angular momentum of light and the transformation of laguerre-gaussian laser modes, *Phys. Rev. A* **45**, 8185 (1992).
- [7] K. G. Lagoudakis, M. Wouters, M. Richard, A. Baas, I. Carusotto, R. André, L. S. Dang, and B. Deveaud-Plédran, Quantized vortices in an exciton–polariton condensate, *Nat. Phys.* **4**, 706 (2008).
- [8] G. Roumpos, M. D. Fraser, A. Löffler, S. Höfling, A. Forchel, and Y. Yamamoto, Single vortex–antivortex pair in an exciton-polariton condensate, *Nat. Phys.* **7**, 129 (2011).
- [9] A. K. Geim, I. V. Grigorieva, S. V. Dubonos, J. G. S. Lok, J. C. Maan, A. E. Filippov, and F. M. Peeters, Phase transitions in individual sub-micrometre superconductors, *Nature* **390**, 259 (1997).
- [10] A. K. Geim, S. V. Dubonos, J. J. Palacios, I. V. Grigorieva, M. Henini, and J. J. Schermer, Fine structure in magnetization of individual fluxoid states, *Phys. Rev. Lett.* **85**, 1528 (2000).
- [11] M. Morelle, J. Bekaert, and V. V. Moshchalkov, Influence of sample geometry on vortex matter in superconducting microstructures, *Phys. Rev. B* **70**, 094503 (2004).
- [12] N. Kokubo, S. Okayasu, A. Kanda, and B. Shinozaki, Scanning squid microscope study of vortex polygons and shells in weak-pinning disks of an amorphous superconducting film, *Phys. Rev. B* **82**, 014501 (2010).
- [13] A. Kanda, B. J. Baelus, F. M. Peeters, K. Kadowaki, and Y. Ootuka, Experimental evidence for giant vortex states in a mesoscopic superconducting disk, *Phys. Rev. Lett.* **93**, 257002 (2004).
- [14] T. Cren, D. Fokin, F. m. c. Debontridder, V. Dubost, and D. Roditchev, Ultimate vortex confinement studied by scanning tunneling spectroscopy, *Phys. Rev. Lett.* **102**, 127005 (2009).
- [15] T. Cren, L. Serrier-Garcia, F. Debontridder, and D. Roditchev, Vortex fusion and giant vortex states in confined superconducting condensates, *Phys. Rev. Lett.* **107**, 097202 (2011).
- [16] M. Timmermans, L. Serrier-Garcia, M. Perini, J. Van de Vondel, and V. V. Moshchalkov, Direct observation of condensate and vortex confinement in nanostructured superconductors, *Phys. Rev. B* **93**, 054514 (2016).
- [17] A. V. Samokhvalov, I. A. Shereshevskii, N. K. Vdovicheva, M. Taupin, I. M. Khaymovich, J. P. Pekola, and A. S. Mel'nikov, Electronic structure of a mesoscopic superconducting disk: Quasiparticle tunneling between the giant vortex core and the disk edge, *Phys. Rev. B* **99**, 134512 (2019).
- [18] F. Ando, Y. Miyasaka, T. Li, J. Ishizuka, T. Arakawa, Y. Shiota, T. Moriyama, Y. Yanase, and T. Ono, Observation of superconducting diode effect, *Nature* **584**, 373 (2020).
- [19] L. Bauriedl, C. Bäuml, L. Fuchs, C. Baumgartner, N. Paulik, J. M. Bauer, K.-Q. Lin, J. M. Lupton, T. Taniguchi, K. Watanabe, C. Strunk, and N. Paradiso,

- Supercurrent diode effect and magnetochiral anisotropy in few-layer NbSe₂, *Nat. Commun.* **13**, 4266 (2022).
- [20] C. Baumgartner, L. Fuchs, A. Costa, S. Reinhardt, S. Gronin, G. C. Gardner, T. Lindemann, M. J. Manfra, P. E. Faria Junior, D. Kochan, J. Fabian, N. Paradiso, and C. Strunk, Supercurrent rectification and magnetochiral effects in symmetric Josephson junctions, *Nat. Nanotechnol.* **17**, 39 (2022).
- [21] H. Wu, Y. Wang, Y. Xu, P. K. Sivakumar, C. Pasco, U. Filippozzi, S. S. P. Parkin, Y.-J. Zeng, T. McQueen, and M. N. Ali, The field-free Josephson diode in a van der Waals heterostructure, *Nature* **604**, 653 (2022).
- [22] K.-R. Jeon, J.-K. Kim, J. Yoon, J.-C. Jeon, H. Han, A. Cottet, T. Kontos, and S. S. P. Parkin, Zero-field polarity-reversible Josephson supercurrent diodes enabled by a proximity-magnetized Pt barrier, *Nat. Mater.* **21**, 1008 (2022).
- [23] M. Nadeem, M. S. Fuhrer, and X. Wang, The superconducting diode effect, *Nat. Rev. Phys.* **5**, 558 (2023).
- [24] S. Ghosh, V. Patil, A. Basu, Kuldeep, A. Dutta, D. A. Jangade, R. Kulkarni, A. Thamizhavel, J. F. Steiner, F. von Oppen, and M. M. Deshmukh, High-temperature Josephson diode, *Nat. Mater.* 10.1038/s41563-024-01804-4 (2024).
- [25] J.-X. Lin, P. Siriviboon, H. D. Scammell, S. Liu, D. Rhodes, K. Watanabe, T. Taniguchi, J. Hone, M. S. Scheurer, and J. I. A. Li, Zero-field superconducting diode effect in small-twist-angle trilayer graphene, *Nat. Phys.* **18**, 1221 (2022).
- [26] B. Pal, A. Chakraborty, P. K. Sivakumar, M. Davydova, A. K. Gopi, A. K. Pandeya, J. A. Krieger, Y. Zhang, M. Date, S. Ju, N. Yuan, N. B. M. Schröter, L. Fu, and S. S. P. Parkin, Josephson diode effect from Cooper pair momentum in a topological semimetal, *Nat. Phys.* **18**, 1228 (2022).
- [27] N. F. Q. Yuan and L. Fu, Supercurrent diode effect and finite-momentum superconductors, *Proc. Natl. Acad. Sci.* **119**, e2119548119 (2022).
- [28] V. M. Edelstein, Magnetoelectric Effect in Polar Superconductors, *Phys. Rev. Lett.* **75**, 2004 (1995).
- [29] S. Ilić and F. S. Bergeret, Theory of the supercurrent diode effect in Rashba superconductors with arbitrary disorder, *Phys. Rev. Lett.* **128**, 177001 (2022).
- [30] A. Daido and Y. Yanase, Superconducting diode effect and nonreciprocal transition lines, *Phys. Rev. B* **106**, 205206 (2022).
- [31] J. J. He, Y. Tanaka, and N. Nagaosa, A phenomenological theory of superconductor diodes, *New J. Phys.* **24**, 053014 (2022).
- [32] B. Turini, S. Salimian, M. Carrega, A. Iorio, E. Strambini, F. Giazotto, V. Zannier, L. Sorba, and S. Heun, Josephson diode effect in high-mobility InSb nanoflags, *Nano Lett.* **22**, 8502 (2022), pMID: 36285780.
- [33] Y. Hou, F. Nichele, H. Chi, A. Lodesani, Y. Wu, M. F. Ritter, D. Z. Haxell, M. Davydova, S. Ilić, O. Glezakou-Elbert, A. Varambally, F. S. Bergeret, A. Kamra, L. Fu, P. A. Lee, and J. S. Moodera, Ubiquitous Superconducting Diode Effect in Superconductor Thin Films, *Phys. Rev. Lett.* **131**, 027001 (2023).
- [34] A. Sundaresh, J. I. Väyrynen, Y. Lyanda-Geller, and L. P. Rokhinson, Diamagnetic mechanism of critical current non-reciprocity in multilayered superconductors, *Nat. Commun.* **14**, 1628 (2023).
- [35] V. M. Krasnov, V. A. Oboznov, and N. F. Pedersen, Fluxon dynamics in long Josephson junctions in the presence of a temperature gradient or spatial nonuniformity, *Phys. Rev. B* **55**, 14486 (1997).
- [36] T. Golod and V. M. Krasnov, Demonstration of a superconducting diode-with-memory, operational at zero magnetic field with switchable nonreciprocity, *Nat. Commun.* **13**, 3658 (2022).
- [37] D. Margineda, A. Crippa, E. Strambini, Y. Fukaya, M. T. Mercaldo, C. Ortix, M. Cuoco, and F. Giazotto, Back-action supercurrent diodes (2023), arXiv:2311.14503.
- [38] T. Golod, A. Rydh, and V. M. Krasnov, Detection of the phase shift from a single Abrikosov vortex, *Phys. Rev. Lett.* **104**, 227003 (2010).
- [39] D. Suri, A. Kamra, T. N. G. Meier, M. Kronseder, W. Belzig, C. H. Back, and C. Strunk, Non-reciprocity of vortex-limited critical current in conventional superconducting micro-bridges, *Appl. Phys. Lett.* **121**, 102601 (2022).
- [40] A. Gutfreund, H. Matsuki, V. Plastovets, A. Noah, L. Gorzawski, N. Fridman, G. Yang, A. Buzdin, O. Millo, J. W. A. Robinson, and Y. Anahory, Direct observation of a superconducting vortex diode, *Nat. Commun.* **14**, 1630 (2023).
- [41] W. Gillijns, A. V. Silhanek, V. V. Moshchalkov, C. J. O. Reichhardt, and C. Reichhardt, Origin of reversed vortex ratchet motion, *Phys. Rev. Lett.* **99**, 247002 (2007).
- [42] J. Jiang, Y.-L. Wang, M. V. Milošević, Z.-L. Xiao, F. M. Peeters, and Q.-H. Chen, Reversible ratchet effects in a narrow superconducting ring, *Phys. Rev. B* **103**, 014502 (2021).
- [43] A. He, C. Xue, and Y.-H. Zhou, Switchable reversal of vortex ratchet with dynamic pinning landscape, *Appl. Phys. Lett.* **115**, 10.1063/1.5100988 (2019).
- [44] D. Margineda, A. Crippa, E. Strambini, Y. Fukaya, M. T. Mercaldo, M. Cuoco, and F. Giazotto, Sign reversal diode effect in superconducting dayem nanobridges, *Commun. Phys.* **6**, 343 (2023).
- [45] F. Paolucci, G. De Simoni, and F. Giazotto, A gate- and flux-controlled supercurrent diode effect, *Appl. Phys. Lett.* **122**, 042601 (2023).
- [46] A. Greco, Q. Pichard, and F. Giazotto, Josephson diode effect in monolithic dc-SQUIDs based on 3D Dayem nanobridges, *Appl. Phys. Lett.* **123**, 092601 (2023).
- [47] J. Lustikova, Y. Shiomi, N. Yokoi, N. Kabeya, N. Kimura, K. Ienaga, S. Kaneko, S. Okuma, S. Takahashi, and E. Saitoh, Vortex rectenna powered by environmental fluctuations, *Nat. Commun.* **9**, 4922 (2018).
- [48] Y. M. Itahashi, T. Ideue, Y. Saito, S. Shimizu, T. Ouchi, T. Nojima, and Y. Iwasa, Nonreciprocal transport in gate-induced polar superconductor SrTiO₃, *Sci. Adv.* **6**, eaay9120 (2020).
- [49] In the Supplemental Material we provide details about the model and the methodology. We present how the supercurrent rectification gets modified for mirror and time-reversal symmetric vortex configurations. We discuss and evaluate the general conditions to maximize the amplitude of the supercurrent rectification for a current phase relation that includes only first and second harmonics. We present the dependence of the first harmonic of the supercurrent by considering the lowest order Cooper pairs tunneling process.
- [50] A. A. Golubov, M. Y. Kupriyanov, and E. Il'ichev, The current-phase relation in Josephson junctions, *Rev. Mod. Phys.* **76**, 411 (2004).

- [51] Y. Tanaka, B. Lu, and N. Nagaosa, Theory of giant diode effect in d -wave superconductor junctions on the surface of a topological insulator, Phys. Rev. B **106**, 214524 (2022).
- [52] B. D. Josephson, Possible new effects in superconductive tunnelling, Phys. Lett. **1**, 251 (1962).
- [53] M. Amundsen, J. A. Ouassou, and J. Linder, Field-free nucleation of antivortices and giant vortices in non-superconducting materials, Phys. Rev. Lett. **120**, 207001 (2018).

Supplemental Material for “Design of supercurrent diode by vortex phase texture”

Yuri Fukaya,¹ Maria Teresa Mercaldo,² Daniel Margineda,³ Alessandro Crippa,³
Elia Strambini,³ Francesco Giazotto,³ Carmine Ortix,² and Mario Cuoco¹

¹*CNR-SPIN, I-84084 Fisciano (SA), Italy, c/o Università di Salerno, I-84084 Fisciano (SA), Italy*

²*Dipartimento di Fisica “E. R. Caianiello”, Università di Salerno, IT-84084 Fisciano (SA), Italy*

³*NEST Istituto Nanoscienze-CNR and Scuola Normale Superiore, I-56127, Pisa, Italy*

In the Supplemental Material, we provide details about the model, the methodology, and the boundary condition. We discuss and evaluate the general conditions to maximize the amplitude of the supercurrent rectification for a current phase relation that includes only first and second harmonics. We present the dependence of the first harmonic of the supercurrent by considering the lowest-order Cooper pairs tunneling process.

I. MODEL HAMILTONIAN AND METHODOLOGY

We present the model and the methodology employed to calculate the Josephson current of the superconducting weak-link in the presence of vortices with different winding number. The Josephson junction is schematically shown in Fig. 1 (a) with the system size given by $L_y \times (L_x^L + L_x^N + L_x^R)$ and the superconducting order parameter $\hat{\Delta}_{L,R} e^{i\varphi_{L,R}}$. Hereafter, L , R , and N stand for the indices of left and right-side superconductors, and the normal metal layer, respectively. The Hamiltonian is written as

$$\hat{\mathcal{H}} = \sum_{\langle x,y;x',y' \rangle} \hat{C}^\dagger(x,y) \hat{H}(x,y;x',y';\varphi) \hat{C}(x',y'), \quad (1)$$

with $\varphi = \varphi_L - \varphi_R$ being the phase difference between the superconducting order parameters in the two sides of the junction and $\mathbf{r} = (x,y)$ indicating the coordinate in the real space. Here, $\langle x,y;x',y' \rangle$ indicates the summation within the nearest-neighbor hopping and $\hat{C}^\dagger(x,y) = [c_{x,y,\uparrow}^\dagger, c_{x,y,\downarrow}^\dagger, c_{x,y,\uparrow}, c_{x,y,\downarrow}]$ denotes the creation operator. Then $\hat{H}(x,y;x',y';\varphi)$ is given by

$$\hat{H}(x,y;x',y';\varphi) = \hat{H}^L(x,y;x',y';\varphi) + \hat{H}^R(x,y;x',y') + \hat{H}^N(x,y;x',y') + \hat{H}_J^L(x,y;x',y) + \hat{H}_J^R(x,y;x',y), \quad (2)$$

with the Hamiltonian in the Nambu space $\hat{H}^{L,N,R}$ that is constructed by the on site energy term \hat{u} , the energy gap function with spin-singlet s -wave state $\hat{\Delta}_{L,R} e^{i\varphi_{L,R}}$, the nearest neighbor hopping terms $\hat{t}_{x,y}$, and the tunneling part $\hat{H}_J^{L,R}$. The local term in the normal state is

$$\hat{u}(x,y) = \begin{pmatrix} -\varepsilon & 0 \\ 0 & -\varepsilon \end{pmatrix}, \quad (3)$$

and the nearest-neighbor hopping,

$$\hat{t}_x(x,y;x+1,y) = \hat{t}_x^\dagger(x,y;x-1,y) = \begin{pmatrix} -t & 0 \\ 0 & -t \end{pmatrix}, \quad (4)$$

$$\hat{t}_y(x,y;x,y+1) = \hat{t}_y^\dagger(x,y;x,y-1) = \begin{pmatrix} -t & 0 \\ 0 & -t \end{pmatrix}. \quad (5)$$

The superconducting order parameter $\hat{\Delta}_{L,R}$ has spin-singlet/ s -wave symmetry in both superconductors:

$$\hat{\Delta}_X(x,y) = \begin{pmatrix} 0 & \Delta_X \\ -\Delta_X & 0 \end{pmatrix}, \quad (6)$$

with $X=L,R$. In the present study, the pairing amplitude is on site and included in the local term of Hamiltonian for the left and right-side superconductors. The tunneling Hamiltonian is expressed as

$$\hat{t}_J(x,y;x+1,y) = \hat{t}_J^\dagger(x,y;x-1,y) = t_{\text{int}} \begin{pmatrix} -t & 0 \\ 0 & -t \end{pmatrix}, \quad (7)$$

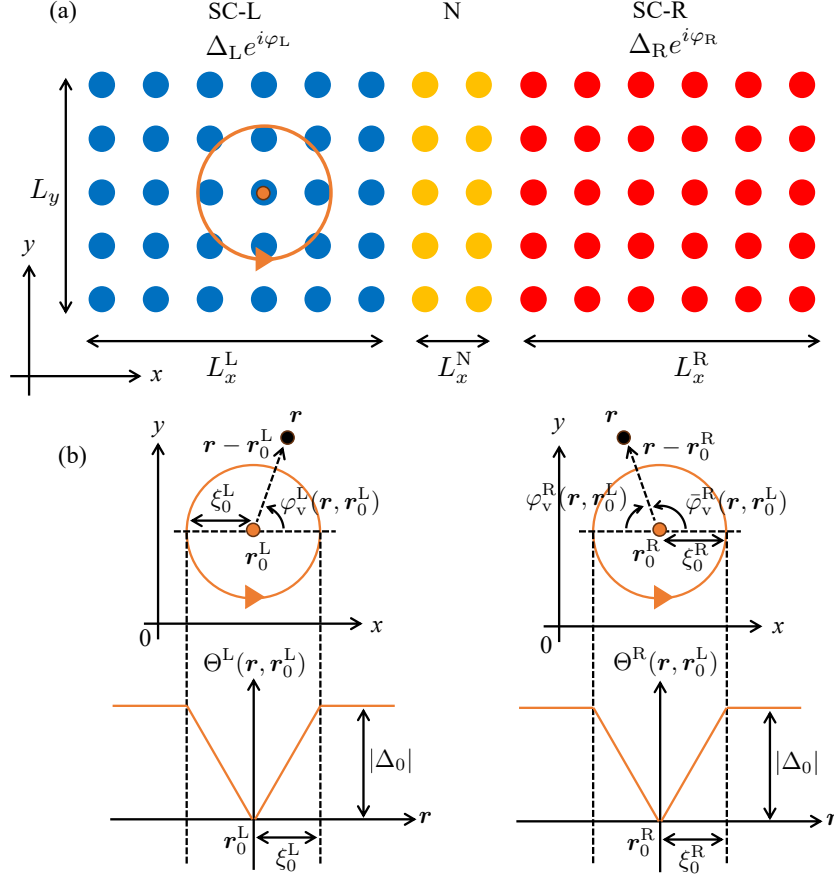


FIG. 1. (a) Sketch of the Josephson junction in the xy -plane. Blue, yellow, and red circles denote the atomic sites in the real space $\mathbf{r} = (x, y)$. The system size in Josephson junctions is set by $L_y \times (L_x^L + L_x^N + L_x^R)$. The orange circle is an example of a phase vortex in superconductors. The blue and red sites indicate the superconducting domain, while the yellow region stands for the normal metal layers. (b) Phase of the vortex $\varphi_v^X(\mathbf{r})$ and corresponding superconducting order parameter $\Theta^X(\mathbf{r})$ in the real space with $X=L,R$. We also show the corresponding notations for the phase vortex for each side. ξ_0 indicates the size of the vortex core whereas the amplitude superconducting order parameter vanishes.

with t_{int} the charge transfer amplitude at the interface setting out the transparency of the junction.

The phase of the superconducting order parameter associated to the vortex configuration is represented in Fig. 1 (b). At the position $\mathbf{r} = (x, y)$, the phase vortex in the left-side superconductor is given by

$$\varphi_v^L(\mathbf{r}, \mathbf{r}_0^L) = V_0^L \arg[(x - x_0^L) + i(y - y_0^L)], \quad (8)$$

with the position of the core $\mathbf{r}_0^L = (x_0^L, y_0^L)$. In a similar way, one can introduce the phase vortex at the core $\mathbf{r}_0^R = (x_0^R, y_0^R)$ in the right-side superconductor as

$$\varphi_v^R(\mathbf{r}, \mathbf{r}_0^R) = \pi - \bar{\varphi}_v^R(\mathbf{r}, \mathbf{r}_0^R), \quad (9)$$

$$\bar{\varphi}_v^R(\mathbf{r}, \mathbf{r}_0^R) = V_0^R \arg[(x - x_0^R) + i(y - y_0^R)], \quad (10)$$

due to the mirror symmetry in the yz -plane. Here, V_0^X denotes the vortex winding.

The pair potential is described as

$$\Delta_X = \begin{cases} \Theta(\mathbf{r}, \mathbf{r}_0^X) e^{i\varphi_v^X(\mathbf{r}, \mathbf{r}_0^X)} & \text{with phase vortex} \\ |\Delta_0| & \text{without phase vortex} \end{cases}, \quad (11)$$

with the energy gap amplitude $|\Delta_0|$. In the former case, the energy gap amplitude $\Theta(\mathbf{r})$ is modified by the position:

$$\Theta^X(\mathbf{r}, \mathbf{r}_0^X) = |\Delta_0| \tilde{\Theta}^X(\mathbf{r}, \mathbf{r}_0^X), \quad (12)$$

$$\tilde{\Theta}^X(\mathbf{r}, \mathbf{r}_0^X) = \tanh \left[\frac{|\mathbf{r} - \mathbf{r}_0^X|}{\xi_0^X} \right], \quad (13)$$

with the size of the vortex ξ_0^X . We set the parameters as $\varepsilon = -0.25t$, $|\Delta_0| = 0.02t$, and $t_{\text{int}} = 0.90$.

We introduce the formulations to calculate the Josephson current for the superconducting weak link. The free energy in a Josephson junction at zero temperature is evaluated as

$$F(\varphi) = \frac{1}{L_y L_x} \sum_{E < 0} E(\varphi), \quad (14)$$

with the total length along the x -direction $L_x = L_x^L + L_x^N + L_x^R$ and along the y -direction L_y . Here, $E(\varphi)$ stands for the eigenvalue of $\hat{H}(x, y; x', y'; \varphi)$. Then, the current phase relation of the Josephson current in this system is evaluated by a variation of the free energy with respect to the phase bias across the junction:

$$I(\varphi) = \frac{2e}{\hbar} \frac{\partial F(\varphi)}{\partial \varphi}. \quad (15)$$

In this study, we adopt the effective coordinate. The reduced coordinates \tilde{x} and \tilde{y} are defined as

$$\tilde{x} = \begin{cases} \frac{x^L}{L_x^L} + \tilde{x}_L^N & \tilde{x} < 0 \\ \frac{x^R}{L_x^R} - \tilde{x}_R^N & \tilde{x} > 0 \end{cases}, \quad (16)$$

$$\tilde{y} = \frac{y}{L_y}, \quad (17)$$

with

$$\tilde{x}_L^N = \frac{L_x^N/2}{L_x^L + L_x^N/2}, \quad (18)$$

$$\tilde{x}_R^N = \frac{L_x^N/2}{L_x^R + L_x^N/2}, \quad (19)$$

and the effective size of the vortex:

$$\begin{aligned} \tilde{\xi}_0^L(x) &= \frac{\xi_0^L}{L_x^L}, & \tilde{\xi}_0^L(y) &= \frac{\xi_0^L}{L_y}, \\ \tilde{\xi}_0^R(x) &= \frac{\xi_0^R}{L_x^R}, & \tilde{\xi}_0^R(y) &= \frac{\xi_0^R}{L_y}. \end{aligned}$$

We also define the effective coordinate for the position of the vortex core as

$$\tilde{x}_0^L = \frac{x_0^L}{L_x^L} + \tilde{x}_L^N, \quad (20)$$

$$\tilde{x}_0^R = \frac{x_0^R}{L_x^R} - \tilde{x}_R^N, \quad (21)$$

$$\tilde{y}_0^{L,R} = \frac{y_0}{L_y}. \quad (22)$$

In this study, we choose the size as $L_x^N = 10$, $L_x^R = L_x^L = aL_y$, $L_y = 30$ with the aspect ratio a , and $\xi_0^L = \xi_0^R = 10$.

In general, one can show that the following relations for the rectification amplitude η holds when considering vortex (arbitrary winding amplitude $V_0 > 0$) or antivortex ($V_0 < 0$) configurations with a given position of the core $(\tilde{x}_0, \tilde{y}_0)$ and mirror related core positions:

$$\eta(\tilde{x}_0, \tilde{y}_0, V_0) = -\eta(-\tilde{x}_0, \tilde{y}_0, V_0), \quad (23)$$

$$\eta(\tilde{x}_0, \tilde{y}_0, V_0) = -\eta(\tilde{x}_0, -\tilde{y}_0, V_0), \quad (24)$$

$$\eta(\tilde{x}_0, \tilde{y}_0, V_0) = -\eta(\tilde{x}_0, \tilde{y}_0, -V_0). \quad (25)$$

Therefore, regarding a combination of mirror and time-reversal symmetries, one can also obtain that a change from vortex to antivortex and of the vortex core position does not alter the sign and amplitude of the rectification:

$$\eta(\tilde{x}_0, \tilde{y}_0, V_0) = \eta(-\tilde{x}_0, \tilde{y}_0, -V_0). \quad (26)$$

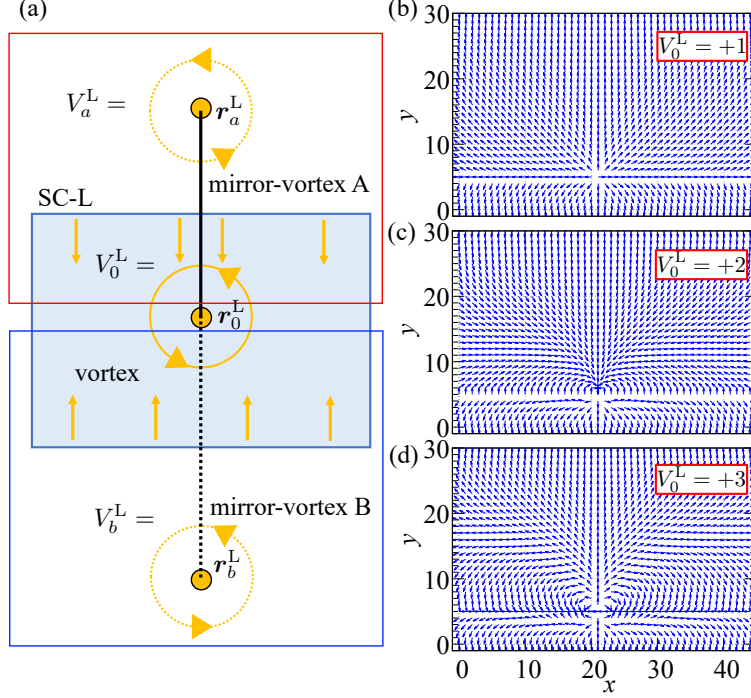


FIG. 2. (a) Schematic illustration for the phase vortex to deal with the boundary condition. We put two mirror vortices outside the left-side superconductor. Phase vortex with the boundary condition in a superconductor at (b) $V_0^L = +1$, (c) $V_0^L = +2$, and (d) $V_0^L = +3$. Vortex core is set at $(x, y) = (21, 6)$ in (b)-(d).

II. VORTEX PHASE TEXTURE WITH THE BOUNDARY CONDITION

In the previous section, we do not consider the boundary condition near the edge along the x -direction. We show the formulation to deal with the boundary condition in our study. As shown in Fig. 2 (a), we suppose a phase vortex in a superconductor and two additional mirror vortices outside a superconductor. For the boundary condition, we replace

$$\varphi_v^L(\mathbf{r}, \mathbf{r}_0^L) \rightarrow \tilde{\varphi}_v^L(\mathbf{r}, \mathbf{r}_0^L), \quad (27)$$

with

$$\tilde{\varphi}_v^L(\mathbf{r}, \mathbf{r}_0^L) = \begin{cases} \varphi_v^L(\mathbf{r}, \mathbf{r}_0^L) + \varphi_a^L(\mathbf{r}, \mathbf{r}_a^L) + (V_0^L - 1)\pi & y > y_0^L + 0.5 \\ \varphi_v^L(\mathbf{r}, \mathbf{r}_0^L) + (V_0^L/2 - 1)\pi & y_0^L - 0.5 \leq y \leq y_0^L + 0.5, \\ \varphi_v^L(\mathbf{r}, \mathbf{r}_0^L) + \varphi_b^L(\mathbf{r}, \mathbf{r}_b^L) + V_0^L\pi & y < y_0^L - 0.5 \end{cases}, \quad (28)$$

$$\varphi_a^L(\mathbf{r}, \mathbf{r}_a^L) = V_a^L \arg[(x - x_a) + i(y - y_a)], \quad (29)$$

$$\varphi_b^L(\mathbf{r}, \mathbf{r}_b^L) = V_b^L \arg[(x - x_b) + i(y - y_b)], \quad (30)$$

where $V_a^L = V_b^L = V_0^L$ are the number of mirror vortices and these core position $\mathbf{r}_{a,b}^L$ are defined as

$$x_a^L = x_0^L, \quad (31)$$

$$y_a^L = (L_y - 1) + L_y - y_0^L - 2, \quad (32)$$

$$x_b^L = x_0^L, \quad (33)$$

$$y_b^L = -y_0^L + 1. \quad (34)$$

We introduce the modulation factors to obtain the continuous phase texture in a superconductor. In Fig. 2 (b)-(d), we plot the phase texture $\mathbf{F} = [f_x(\mathbf{r}, \mathbf{r}_0^L), f_y(\mathbf{r}, \mathbf{r}_0^L)]$ with

$$f_x(\mathbf{r}, \mathbf{r}_0^L) = -\sin \tilde{\varphi}_v^L(\mathbf{r}, \mathbf{r}_0^L), \quad (35)$$

$$f_y(\mathbf{r}, \mathbf{r}_0^L) = \cos \tilde{\varphi}_v^L(\mathbf{r}, \mathbf{r}_0^L), \quad (36)$$

in a superconductor at (b) $V_0^L = +1$, (c) $+2$, and (d) $+3$. In the presence of two mirror vortices, we obtain $J_y(1) = J(29) = 0$ with

$$J_y(y) = f_y(y) - f_y(y-1), \quad (37)$$

as the boundary condition.

III. CONDITION TO MAXIMIZE THE AMPLITUDE OF THE SUPERCURRENT RECTIFICATION

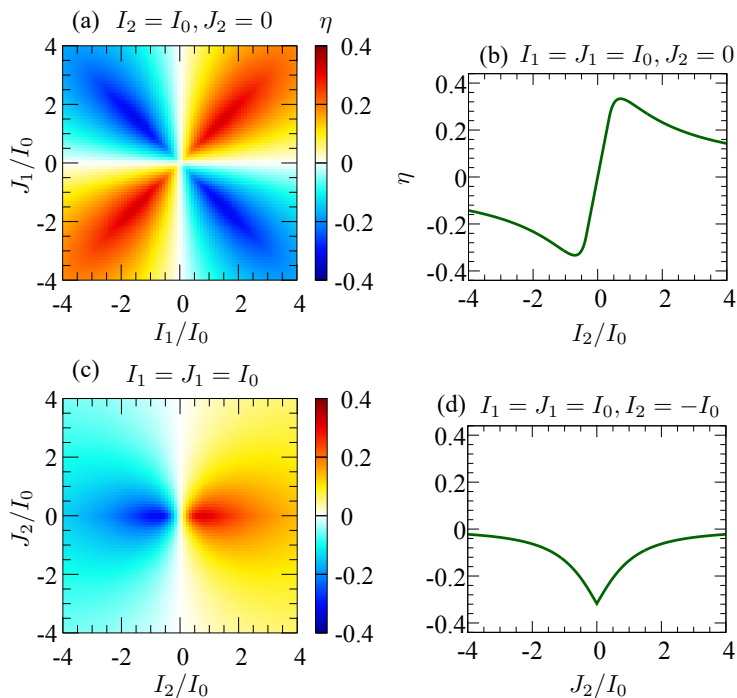


FIG. 3. Rectification η of $I(\varphi) = I_1 \sin \varphi + I_2 \sin 2\varphi + J_1 \cos \varphi + J_2 \cos 2\varphi$ (a) for (I_1, J_1) space and (b) as a function of I_2 . We fix the parameters as (a) $(I_2, J_2) = (I_0, 0)$, (b) $(I_1, J_1, J_2) = (I_0, I_0, 0)$, (c) $(I_1, J_1) = (I_0, I_0)$, and (d) $(I_1, J_1, I_2) = (I_0, I_0, -I_0)$.

In this section, we calculate the optimal conditions to maximize the supercurrent rectification starting from a generic current phase relation that includes the first harmonics (even and odd parity) and the second harmonic (odd parity). Let us then assume the following current phase relation:

$$I(\varphi) = I_1 \sin \varphi + I_2 \sin 2\varphi + J_1 \cos \varphi + J_2 \cos 2\varphi.$$

In order to find the optimal regimes for maximal rectification, one can evaluate η as a function of the amplitudes I_1 , I_2 , and J_1 . First, we calculate η for (I_1, J_1) at $(I_2, J_2) = (I_0, 0)$ in Fig. 3 (a). The maximum value of $|\eta|$ appears around $|I_1| = |J_1| \sim I_0$. Based on this point, we also calculate η as a function of I_2 at $(I_1, J_1, J_2) = (I_0, I_0, 0)$ [Fig. 3 (b)]. The amplitude of η is enhanced around $I_2 = \pm 0.5I_0$. Likewise, to show the role of J_2 , we calculate η for (I_2, J_2) at $(I_1, J_1 = (I_0, I_0))$ in Fig. 3 (c). η is maximized around $J_2 \sim 0$ for $|I_2| \sim I_0$. We also calculate η for J_2 at $(I_1, J_1, I_2) = (I_0, I_0, -I_0)$ [Fig. 3 (d)]. The maximum $|\eta|$ appears at $I_2 = 0$. Thus, both $|I_1|$ and $|J_1|$ should be comparable with $|I_2|$ and $|J_2|$ should be minimized to maximize the rectification in Josephson current.

IV. EVALUATION OF FIRST-HARMONIC COMPONENT OF SUPERCURRENT

The first-harmonic components of the Josephson current at a position \mathbf{r} can be estimated by considering the direct Cooper pair tunneling process as

$$j(\varphi; \mathbf{r}, \mathbf{r}_0^L) \propto \text{Im}[\Delta_L(\mathbf{r}, \mathbf{r}_0^L)\Delta_R^*], \quad (38)$$

where \mathbf{r}_0^L is the position of a vortex core in the left-side superconductor. By expanding the expression for $j(\phi)$ we obtain

$$\begin{aligned} j(\varphi; \mathbf{r}, \mathbf{r}_0^L) &\propto \text{Im} \left[|\Delta_0|^2 \tanh \left[\frac{|\mathbf{r} - \mathbf{r}_0^L|}{\xi_0^L} \right] e^{i(\varphi_L - \varphi_R)} e^{i\tilde{\varphi}_v^L(\mathbf{r}, \mathbf{r}_0^L)} \right] \\ &= |\Delta_0| \sin \varphi \tanh \left[\frac{|\mathbf{r} - \mathbf{r}_0^L|}{\xi_0^L} \right] \cos \tilde{\varphi}_v^L(\mathbf{r}, \mathbf{r}_0^L) d\mathbf{r} + |\Delta_0| \cos \varphi \tanh \left[\frac{|\mathbf{r} - \mathbf{r}_0^L|}{\xi_0^L} \right] \sin \tilde{\varphi}_v^L(\mathbf{r}, \mathbf{r}_0^L) d\mathbf{r}, \end{aligned} \quad (39)$$

with $\varphi = \varphi_L - \varphi_R$. The resulting first-harmonic Josephson current can be described by the spatial average of $j(\varphi; \mathbf{r}, \mathbf{r}_0^L)$ over the area of the superconducting leads:

$$\begin{aligned} \tilde{I}(\varphi; \mathbf{r}_0^L) &= \int_{S_L} j(\mathbf{r}, \mathbf{r}_0^L) d\mathbf{r} \\ &\propto \sin \varphi \int_{S_L} \tanh \left[\frac{|\mathbf{r} - \mathbf{r}_0^L|}{\xi_0^L} \right] \cos \tilde{\varphi}_v^L(\mathbf{r}, \mathbf{r}_0^L) d\mathbf{r} + \cos \varphi \int_{S_L} \tanh \left[\frac{|\mathbf{r} - \mathbf{r}_0^L|}{\xi_0^L} \right] \sin \tilde{\varphi}_v^L(\mathbf{r}, \mathbf{r}_0^L) d\mathbf{r}, \end{aligned} \quad (40)$$

with S_L being the area of the left-side superconductor. Based on this analysis, we get that

$$\tilde{I}(\varphi; \mathbf{r}_0^L) \propto F_c(\mathbf{r}_0^L) \sin \varphi + F_s(\mathbf{r}_0^L) \cos \varphi, \quad (41)$$

with

$$F_{c1}(\mathbf{r}_0^L) = \int_{S_L} \tanh \left[\frac{|\mathbf{r} - \mathbf{r}_0^L|}{\xi_0^L} \right] \cos \tilde{\varphi}_v^L(\mathbf{r}, \mathbf{r}_0^L) d\mathbf{r}, \quad (42)$$

$$F_{s1}(\mathbf{r}_0^L) = \int_{S_L} \tanh \left[\frac{|\mathbf{r} - \mathbf{r}_0^L|}{\xi_0^L} \right] \sin \tilde{\varphi}_v^L(\mathbf{r}, \mathbf{r}_0^L) d\mathbf{r}, \quad (43)$$

where S is the area of the superconducting lead.

For completeness, we also note that the second harmonic Josephson current can be evaluated by considering the second-order Cooper pair tunneling processes:

$$\begin{aligned} \tilde{I}_2(\varphi; \mathbf{r}_0^L) &\propto \int_S \text{Im}[\Delta_L(\mathbf{r}, \mathbf{r}_0^L)\Delta_R^*\Delta_L(\mathbf{r}, \mathbf{r}_0^L)\Delta_R^*] d\mathbf{r} \\ &= |\Delta_0|^4 \sin 2\varphi \int_S \tanh^2 \left[\frac{|\mathbf{r} - \mathbf{r}_0^L|}{\xi_0^L} \right] \cos 2\tilde{\varphi}_v^L(\mathbf{r}, \mathbf{r}_0^L) d\mathbf{r} + |\Delta_0|^4 \cos 2\varphi \int_S \tanh^2 \left[\frac{|\mathbf{r} - \mathbf{r}_0^L|}{\xi_0^L} \right] \sin 2\tilde{\varphi}_v^L(\mathbf{r}, \mathbf{r}_0^L) d\mathbf{r}. \end{aligned} \quad (44)$$

Then, we can also find

$$F_{c2}(\mathbf{r}_0^L) = |\Delta_0|^4 \int_S \tanh^2 \left[\frac{|\mathbf{r} - \mathbf{r}_0^L|}{\xi_0^L} \right] \cos 2\tilde{\varphi}_v^L(\mathbf{r}, \mathbf{r}_0^L) d\mathbf{r}, \quad (45)$$

$$F_{s2}(\mathbf{r}_0^L) = |\Delta_0|^4 \int_S \tanh^2 \left[\frac{|\mathbf{r} - \mathbf{r}_0^L|}{\xi_0^L} \right] \sin 2\tilde{\varphi}_v^L(\mathbf{r}, \mathbf{r}_0^L) d\mathbf{r}, \quad (46)$$

for $\bar{I}_2(\mathbf{r}_0^L)$ and $\bar{J}_2(\mathbf{r}_0^L)$, respectively. Since both I_2 and J_2 are the $|\Delta_0|^4$ order, they are generally smaller in amplitude than I_1 and J_1 , as they are proportional to $|\Delta_0|^2$. Then, close to the nodal lines of the first harmonics, the second harmonic components are comparable in amplitude.

V. SUPERCURRENT RECTIFICATION AND SYSTEM SIZE

We consider the dependence of the system size in the Josephson current. In the main text we have reported the simulation for the case Figure 4 shows the rectification and the corresponding components of the Josephson current I_1 , I_2 , J_1 , and J_2 for $V^L = +1$ at $\tilde{x}_0^L = -0.52$ with the system size $L_x^L = L_x^R = 66$, $L_x^N = 10$, $L_y = 44$, and $\xi_0^L = 15$. As compared with Fig. 2 (b)(d) with the smaller system size, the amplitude of the rectification is almost the same. Thus, our calculation is independent of the system size.

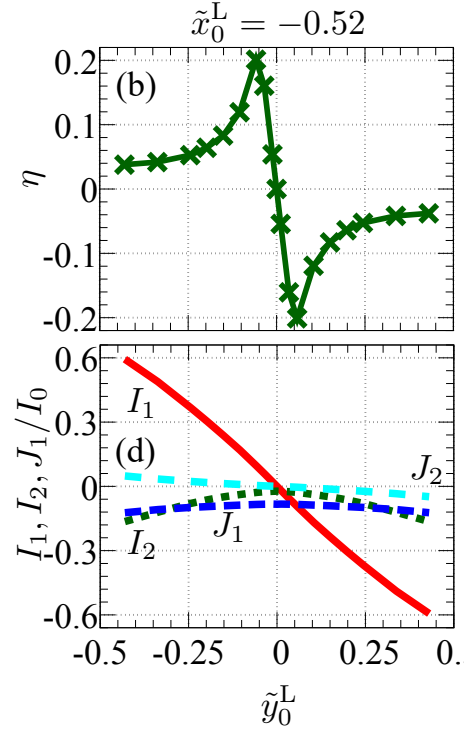


FIG. 4. (a) Rectification and (b) corresponding components of Josephson current I_1 , I_2 , J_1 , and J_2 for $V_0^L = +1$ at $\tilde{x}_0^L = -0.52$. We choose system size as $L_x^L = L_x^R = 66$, $L_x^N = 10$, $L_y = 44$, and $\xi_0^L = 15$. Red, green, blue, and cyan lines indicate I_1 , I_2 , J_1 , and J_2 , respectively.

VI. SUPERCURRENT RECTIFICATION: TWO VORTICES IN A SUPERCONDUCTOR

We show the rectification caused by two vortices in one lead of the superconducting junction. The pair potential with two vortices in the left-side superconductor is expressed by:

$$\Delta_L = |\Delta_0| \prod_j \tilde{\Theta}_j(\mathbf{r}) e^{i\varphi_{v_j}^L(\mathbf{r})}, \quad (47)$$

with

$$\tilde{\Theta}_j(\mathbf{r}) = \tanh \left[\frac{|\mathbf{r} - \mathbf{r}_j^L|}{\xi_j^L} \right], \quad (48)$$

the size of vortices ξ_j^L , and the core positions $\mathbf{r}_j^L = (x_j^L, y_j^L)$ for $j = 0, 1$. Each phase vortex is given by

$$\varphi_{v_j}^L(\mathbf{r}) = V_j^L \arg[(x - x_j^L) + i(y - y_j^L)], \quad (49)$$

where V^j is the number of winding.

We plot the rectification and Josephson components (I_1 , I_2 , and J_1) as a function of the lateral direction \tilde{y}_1^L in a representative case [Fig 5]. Then we set the position of one phase vortex at $(\tilde{x}_0^L, \tilde{y}_0^L) = (-0.68, 0.017)$. We choose each winding number as Fig. 5 (b,d) $(V_0^L, V_1^L) = (+1, +1)$ and (c,e) $(V_0^L, V_1^L) = (+1, -1)$. For $(V_0^L, V_1^L) = (+1, +1)$, the rectification is enhanced up to 40% near $\tilde{y}_1^L = 0$ [Fig. 5 (b)] owing to the comparable Josephson components $|I_1| \sim |I_2| \sim |J_1|$ [Fig. 5 (d)]. On the other hand, for $(V_0^L, V_1^L) = (+1, -1)$, because $|I_1|$ is larger than $|I_2|$ and $|J_1|$ [Fig. 5 (e)], the amplitude of the rectification is small compared with that for $(V_0^L, V_1^L) = (+1, +1)$ [Fig. 5 (c)]. Thus, the same sign for winding is favorable for enhancing the rectification.

Based on the discussion in Sect. IV of Supplemental Materials, we can also define \bar{I}_1 and \bar{J}_1 in this case. $\bar{I}_1(\mathbf{r}_0^L, \mathbf{r}_1^L)$

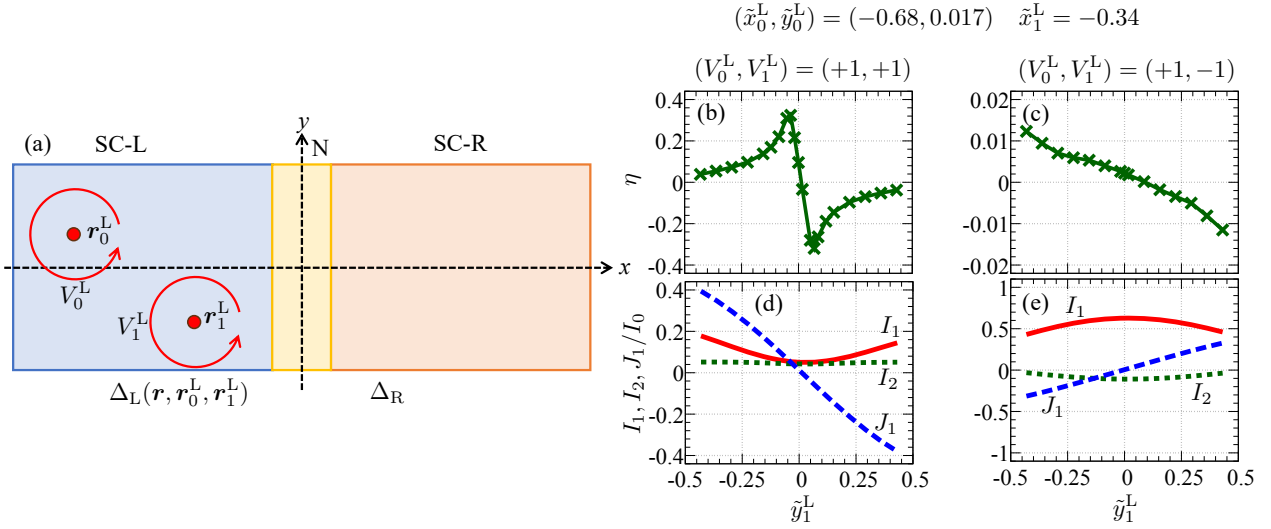


FIG. 5. (a) Schematic illustration for two vortices in the left-side superconductor. (b,c) Rectification η and (d,e) I_1 , I_2 , J_1 as a function of the lateral direction \tilde{y}_1^L for (b,d) $(V_0^L, V_1^L) = (+1, +1)$ and (c,e) $(V_0^L, V_1^L) = (+1, -1)$. We set the core positions as $(\tilde{x}_0^L, \tilde{y}_0^L) = (-0.68, 0.017)$ and $\tilde{x}_1^L = -0.34$ ($L_x^L = L_x^R = 45$, $L_x^N = 10$, $L_y = 30$, $\xi_0^L = \xi_1^L = 10$). $I_0 = 0.122$ stands for the maximum Josephson current without any phase vortices in superconductors.

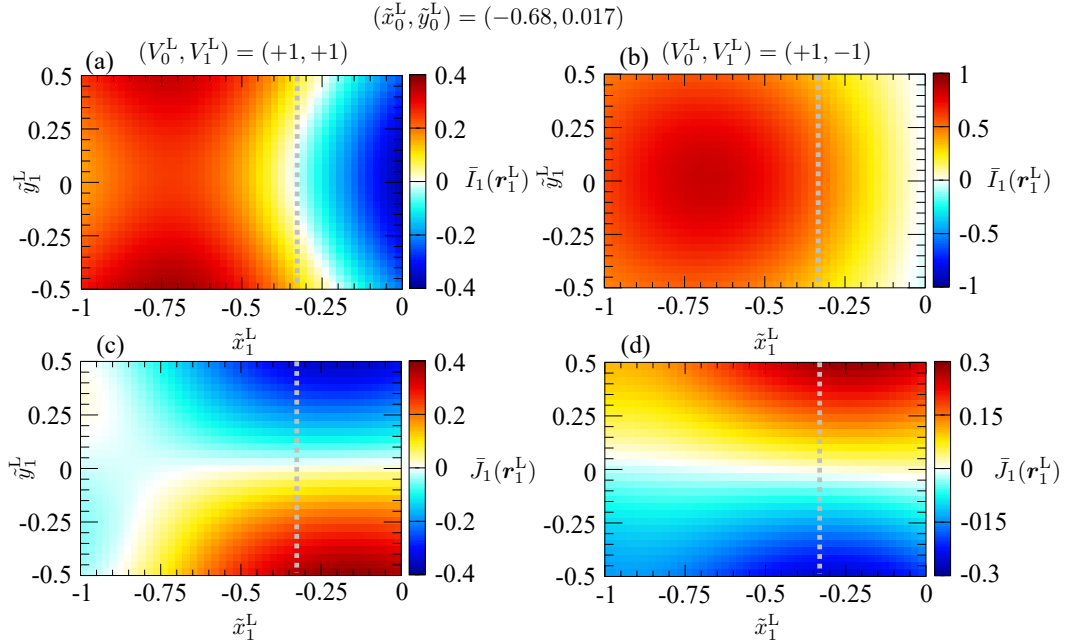


FIG. 6. (a,b) \bar{I}_1 and (c,d) \bar{J}_1 for the \mathbf{r}_1^L space at (a,c) $(V_0^L, V_1^L) = (+1, +1)$ and (b,d) $(V_0^L, V_1^L) = (+1, -1)$. We set the core positions as $(\tilde{x}_0^L, \tilde{y}_0^L) = (-0.68, 0.017)$ and $\tilde{x}_1^L = -0.34$ ($L_x^L = 45$ and $L_y = 30$). The Gray line indicates the scanning position in Fig. 5.

and $\bar{J}_1(\mathbf{r}_0^L, \mathbf{r}_1^L)$ are given by

$$\bar{I}_1(\mathbf{r}_0^L, \mathbf{r}_1^L) = \int_S \cos \varphi_v^L(\mathbf{r}, \mathbf{r}_0^L, \mathbf{r}_1^L) d\mathbf{r}, \quad (50)$$

$$\bar{J}_1(\mathbf{r}_0^L, \mathbf{r}_1^L) = \int_S \sin \varphi_v^L(\mathbf{r}, \mathbf{r}_0^L, \mathbf{r}_1^L) d\mathbf{r}, \quad (51)$$

with $\varphi_v^L(\mathbf{r}, \mathbf{r}_0^L, \mathbf{r}_1^L) = \varphi_{v_0}^L(\mathbf{r}, \mathbf{r}_0^L) + \varphi_{v_1}^L(\mathbf{r}, \mathbf{r}_1^L)$. Fixing the position of one phase vortex at $(\tilde{x}_0^L, \tilde{y}_0^L) = (-0.68, 0.017)$, we plot $\bar{I}_1(\mathbf{r}_0^L, \mathbf{r}_1^L)$ and $\bar{J}_1(\mathbf{r}_0^L, \mathbf{r}_1^L)$ for the \mathbf{r}_1^L space as shown in Fig. 6. For $(V_0^L, V_1^L) = (+1, +1)$ shown in Fig. 6 (a,c),

since nodal lines appear around $\tilde{x}_1^L \sim -0.25$ for \bar{I}_1 and $\tilde{y}_1^L \sim 0$ for J_1 , the amplitude of I_1 and J_1 are small near these lines, respectively. For $(V_0^L, V_1^L) = (+1, -1)$, we obtain $\bar{I}_1 \leq 0$ and the nodal line around $\tilde{y}_1^L \sim 0$ for J_1 [Fig. 6 (b,d)]. Based on these \bar{I}_1 and J_1 , $|I_1|$ is larger than I_1 and J_1 [Fig. 5 (d)]. Thus, using \bar{I}_1 and J_1 is generic way to express I_1 and J_1 .